

Three-Dimensional Crumpled Reduced Graphene Oxide/MoS₂ Nanoflowers: A Stable Anode for Lithium-Ion Batteries

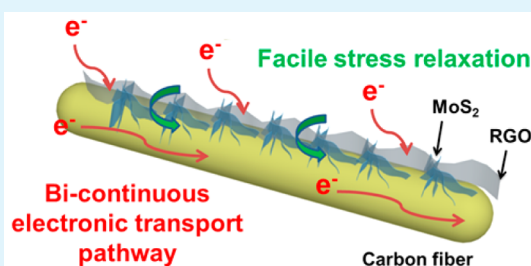
Fangyu Xiong,[†] Zhengyang Cai,[†] Longbing Qu, Pengfei Zhang, Zefang Yuan, Owusu Kwadwo Asare, Wangwang Xu, Chao Lin, and Liqiang Mai*

State Key Laboratory of Advanced Technology for Materials Synthesis and Processing, Wuhan University of Technology, Wuhan 430070, China

Supporting Information

ABSTRACT: Recently, layered transition-metal dichalcogenides (TMDs) have gained great attention for their analogous graphite structure and high theoretical capacity. However, it has suffered from rapid capacity fading. Herein, we present the crumpled reduced graphene oxide (RGO) decorated MoS₂ nanoflowers on carbon fiber cloth. The three-dimensional framework of interconnected crumpled RGO and carbon fibers provides good electronic conductivity and facile strain release during electrochemical reaction, which is in favor of the cycling stability of MoS₂. The crumpled RGO decorated MoS₂ nanoflowers anode exhibits high specific capacity (1225 mAh/g) and excellent cycling performance (680 mAh/g after 250 cycles). Our results demonstrate that the three-dimensional crumpled RGO/MoS₂ nanoflowers anode is one of the attractive anodes for lithium-ion batteries.

KEYWORDS: lithium-ion battery, crumpled reduced graphene oxide, MoS₂, nanoflower, stable anode



High energy density and power density lithium-ion batteries (LIBs) are widely developed to meet the demand for a variety of energy consumptions such as portable electronic devices, hybrid electric vehicles, electric vehicles, and large-scale energy storage devices.^{1–3} However, the relatively low specific capacity of graphite (372 mAh/g), the commercial anode material, has limited the energy density for LIBs.^{4–6} Therefore, alternative anode materials with high capacity need to be exploited.^{7–10}

Molybdenum disulfide (MoS₂), as one of the typical layered transition-metal dichalcogenides (TMDs), exhibits unique chemical peculiarities based on its layer structure: hexagonal layers of Mo are sandwiched between two S layers, Mo–S combined by strong covalent bonding while S–S interacted by weak van der Waals forces.^{11,12} This graphite-like structure permits lithium ions intercalate into the layers and react with MoS₂ according to the conversion reaction: MoS₂ + 4Li⁺ + 4e[–] = Mo + 2Li₂S, and high lithium storage capacity (about 1000 mAh/g) has been obtained in previous reports.^{13–15} However, it suffers from poor cycling stability, because of the poor electronic conductivity and the large volume change of conversion reaction-based materials during charge/discharge.^{16–19}

To date, strategies like exfoliation methods,^{11,13,20} morphology control,^{14,16,21,22} and conductive decoration^{12,18,23,24} have been adopted by scientists to improve the electronic conductivity and buffer the huge volume variation. Especially, compositing anodes with carbonaceous materials is an efficient approach for improving the cycling stability due to the superior electronic conductivity and mechanical stability of carbonaceous

materials.^{25–30} Furthermore, graphene decorated hybrid nanostructures offer great advantages because of its superior mechanical flexibility and electrical conductivity.^{13,17,31} Recently, our group reported the crumpled graphene encapsulated three-dimensional Ni₃S₂ electrodes through a contraction-strain-driven crumpling method, which display significant improvement in cycling stability.³²

Herein, to integrate all these merits and improve the electrochemical performance of MoS₂, first, we rationally designed and synthesized MoS₂ nanoflowers on carbon fiber cloth (MS) through a facile and scalable hydrothermal method followed by heat treatment. The MoS₂ nanoflowers anode exhibits high reversible capacity and excellent cycling property at low current density while it still suffer from rapid capacity fading at high currents. For this issue, the graphene oxide suspension is introduced (Figure 1). As a result, the crumpled RGO/MoS₂ nanoflowers on carbon cloth (MS-CG) has been obtained, which delivers enhanced rate performance and cycling property. In MS-CG, the framework which is consisted of the crumpled RGO and the carbon fiber provides bicontinuous electron transport paths and efficient ions diffusion distances for the MoS₂ nanoflower (Figure 2a). In addition, the crumpled RGO with great mechanical property facilitates the release of stress caused by repeated volume changes and maintains the integrity of the electrode materials.³² Thus, the high reversible capacity and excellent cycling

Received: April 6, 2015

Accepted: June 3, 2015

Published: June 3, 2015

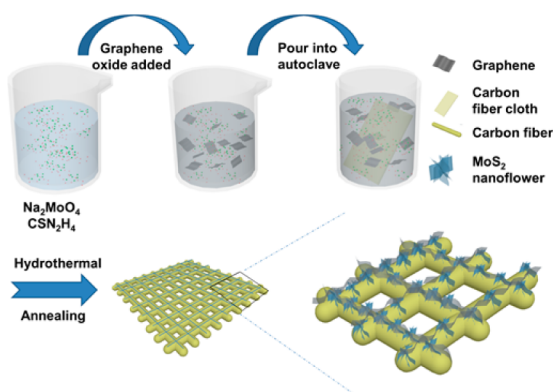


Figure 1. Schematic illustration for the synthesis of RGO decorated MoS_2 nanoflowers on carbon fiber cloth.

performance would be realized based on the crumpled RGO/ MoS_2 /carbon fiber three-dimensional conductive framework.

The crystal structure of the samples is determined by X-ray diffraction (XRD). The precursor without heat treatment is 2H- MoS_2 with large interlayer spacing and low crystallinity (Figure S1a in the Supporting Information).³³ The XRD patterns of MS, MS-CG and plain RGO/ MoS_2 nanoflowers (MS-PG) (Figure 2b) are indexed to hexagonal MoS_2 (JCPDS Card No. 37-1492, 2H form, $a = b = 3.1612 \text{ \AA}$, $c = 12.2985 \text{ \AA}$, $\beta = 120^\circ$), and the corresponding crystal structure is shown in Figure S2 in the Supporting Information.^{15,34} The full width at half-maximum (fwhm) of (002) peak in the three XRD patterns are 1.28, 1.27, and 1.27, respectively, indicating the similar crystallinity of MoS_2 in the MS, MS-PG, and MS-CG. The similarity of the MS and MS-CG in XRD demonstrates that the RGO solution has little effect on the nucleation and crystal growth of MoS_2 nanoflower in the hydrothermal reaction process. Raman spectra of the carbon fiber and MS-CG are given in Figure 2c. The Raman spectra contains the longitudinal

acoustic phonons at M point (LA (M)) due to the electron-phonon coupling,^{13,35} the E1 2g peak at 379 cm^{-1} due to the in-plane opposite vibration of the S atoms based on Mo atom, and the A_{1g} peak at 406 cm^{-1} comes from the out of plane opposite vibration of the S atoms.³⁵ The D band and G band of RGO are overlapped with those of carbon fiber, making them difficult to identify (Figure 2c). The 2D band, D+G band, and 2G band are observed in both pristine carbon cloth and MS-CG (Figure 2c inset). Figure 2d shows the X-ray photoelectron spectroscopy (XPS) survey of as-prepared sample containing Mo, S, C and O elements, whereas the oxygen comes from the functional groups on carbon fiber and RGO.^{29,36} This phenomenon has also been observed in the previous literature.²⁹ The C 1s peak is composed of two components: the C-C at 284.8 eV and the C-O at 286.2 eV, which also demonstrates the existence of oxygen (Figure S3 in the Supporting Information).³⁶ The high-resolution spectrum of S_{2p} peak is resolved into two components located at 162.3 and 163.4 eV, representing the divalent sulfide ions (Figure 2e). The Mo_{3d} peak consists of two sub peaks located at 229.4 and 232.6 eV, corresponding to the Mo^{4+} in MoS_2 (Figure 2f).³⁰

The morphology of MS, MS-PG, and MS-CG is characterized by the field emission scanning electron microscopy (FESEM). Figure 3a shows that MoS_2 nanoflowers uniformly grow on the carbon fiber (Figure 3a). The MoS_2 nanoflowers are average 500 nm in size and composed of lots of ultrathin nanosheets with thickness of about 10 nm (Figure 3b). Remarkably, the precursor of MS shows a similar morphology (Figure S1b in the Supporting Information), indicating the heat treatment has little influence on the morphology. Besides, the RGO in MS-CG and MS-PG is introduced via hydrothermal method and postelectrochemical deposition, respectively. The morphology of MoS_2 nanoflowers on the carbon fibers is not affected by the introduction of RGO (Figure 3c). The RGO in MS-CG crumples and covers the MoS_2 nanoflowers homogeneously. However, in the MS-PG, the RGO nanosheets on the

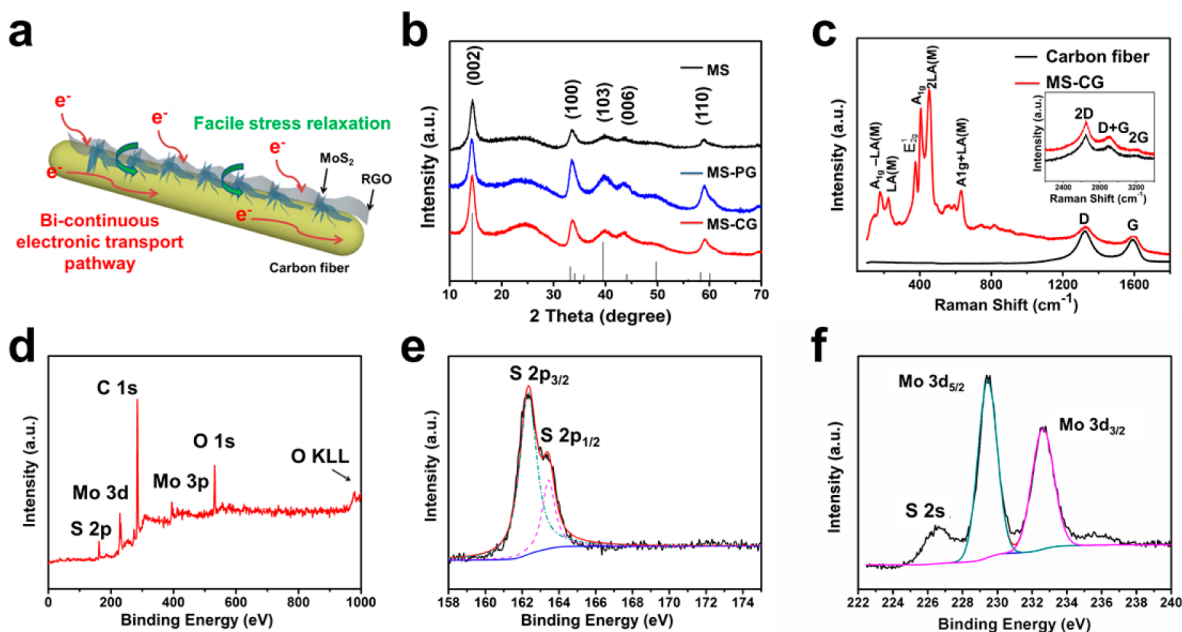


Figure 2. (a) Schematic illustration of the MS-CG composites with bicontinuous electronic transport pathway and facile stress relaxation during charge/discharge process. (b) XRD patterns of MS, MS-PG, and MS-CG. (c) Raman spectra of the carbon fiber and MS-CG. (d–f) XPS spectra of MS-CG: (d) whole XPS spectrum, (e) S_{2p} XPS spectrum, and (f) Mo_{3d} XPS spectrum.

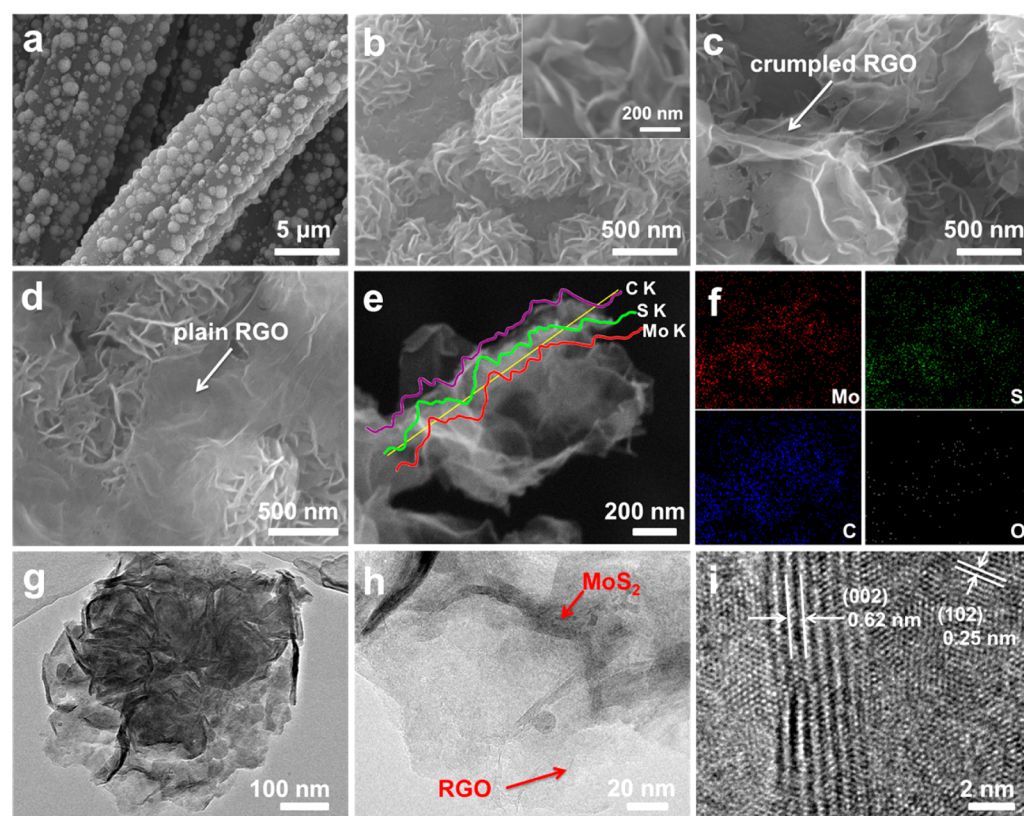


Figure 3. (a) Typical low-magnification FESEM image of MS. (b–d) High magnification FESEM images of (b) MS, (c) MS-CG, and (d) MS-PG. (e) FESEM image with elemental line scanning and (f) elemental mappings of MS-CG. (g–h) TEM images of (g) an individual MS-CG particle and (h) a magnified area of the MS-CG. (i) HRTEM image of the MS-CG.

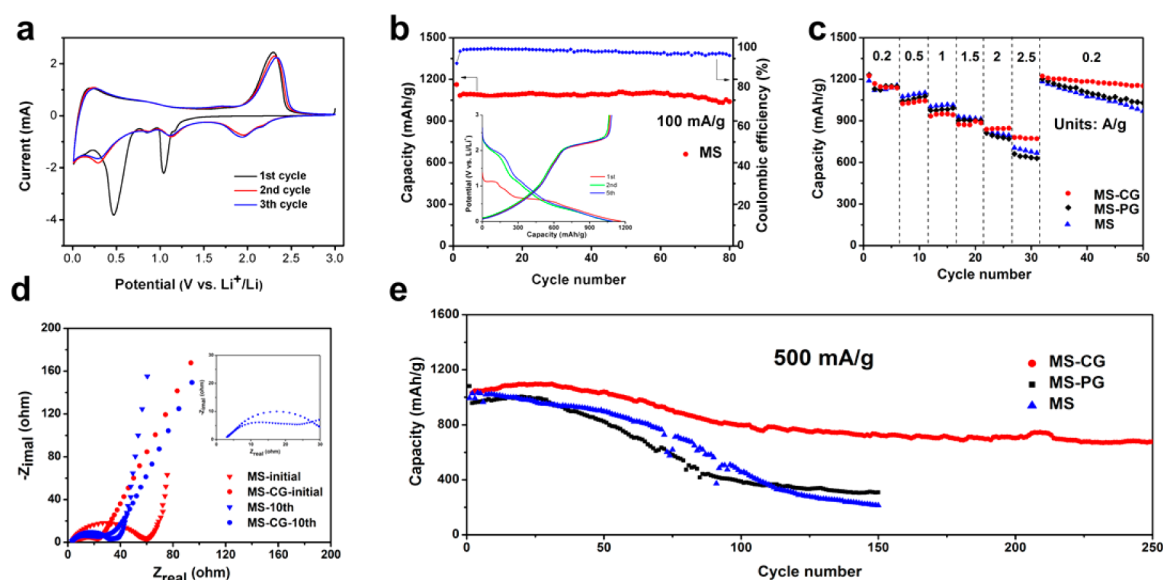


Figure 4. (a) CV curves of the first three cycles of MS at a scan rate of 0.1 mV/s. (b) Cycling performance and Coulombic efficiency of the MS at 100 mA/g, inset shows the corresponding galvanostatic charge–discharge profiles. (c) Rate capability of the MS, MS-PG and MS-CG at the current densities ranging from 0.2 to 2.5 A/g. (d) Nyquist plots of MS and MS-CG before cycling and after 10 cycles. (e) Cycling performance of the MS, MS-PG, and MS-CG at 500 mA/g.

surface of MoS₂ nanoflowers are generally plain (Figure 3d). Figure 3e, f shows the energy-dispersive spectroscopy (EDS) line scanning and elemental mappings of the MS-CG, which give a strong evidence of the homogeneous distribution of Mo, S, and C elements in the crumpled RGO decorated MoS₂ nanoflowers. Transmission electron microscopy (TEM) image

of the MS-CG clearly shows the nanoflower with crumpled RGO (Figure 3g). Magnified TEM image further identifies the adhesion of thin RGO and MoS₂ nanosheet (Figure 3h). The high-resolution TEM (HRTEM) image (Figure 3i) intuitively demonstrates the clear lattice fringes with spaces of 0.62 and

0.25 nm, corresponding to *d*-spaces of (002) and (102) planes in hexagonal MoS₂, respectively.

To evaluate the electrochemical performance, we assembled coin cells (lithium metal as anode) based on the MS-CG, MS-PG, and MS and tested in the voltage range of 0.01–3.00 V versus Li⁺/Li. Figure 4a shows the cyclic voltammogram (CV) curves of the first three cycles of the MS at a scan rate of 0.1 mV/s. In the first cathodic scan, the intensity peak located at 1.04 V is attributed to the intercalation of Li ions into the MoS₂ layers and the formation of 1T Li_xMoS₂.^{37,38} The obvious peak centered at 0.48 V is assigned to the reduction of Mo⁴⁺ to Mo.^{38,39} The broad peak appeared at 0.85 V is caused by the insertion of additional lithium ions into the MoS₂ lattice or the defect sites in MoS₂.^{15,40} For the subsequent anodic scan, the peak located at 2.29 V is assigned to the oxidation of Li₂S to S. For the second cathodic process, the two peaks at 1.96 and 2.16 V correspond to the conversion from S₈ to polysulfides and then to Li₂S, respectively.⁴¹ The other two peaks at 0.30 and 1.13 V correspond to the association between Li and Mo.⁴⁰ As for the MS-CG and MS-PG, the CV profiles (Figure S4 in the Supporting Information) are similar to that of the MS, indicating that the added RGO does not change the electrochemical reaction in the electrode.

Figure 4b shows the cycling performance of MS at current density of 100 mA/g. The initial discharge capacity of the MS anode is as high as 1163 mAh/g. A capacity of 1052 mAh/g is retained even after 80 cycles, corresponding to a capacity retention of 90.5%. This cycling stability is better than that of the previous reported nanosheet-assembled flowerlike MoS₂ particles with size of 700–900 nm (capacity retention of 50.4% after 70 cycles at 100 mA/g),⁴² indicating the carbon fibers are in favor of the cycling stability. The carbon fibers prevent the MoS₂ nanoflowers from aggregation and provide the continuous electronic transport network. The corresponding charge/discharge curves are given in the inset of Figure 4b. In the first discharge profile, two extinct plateaus located at 1.1 and 0.6 V are assigned to the intercalation of lithium ion and the conversion reaction, respectively. In the subsequent charge/discharge processes, the apparent plateaus between 2.0 and 2.4 V correspond to the transforming between Li₂S and S, consistent with the CV curves. The irreversible capacity loss (about 80 mAh/g) in the first cycle is attributed to the formation of solid electrolyte interface (SEI) film and insertion of Li⁺ ions into the defect sites of MoS₂.^{15,40} For the subsequent cycles, the curves overlap well, indicating the good reversibility of MS.

To confirm the effects of crumpled RGO and plain RGO on electrochemical performance, we investigated the rate capability and long-term cycling stability of MS, MS-CG, and MS-PG. The MS-CG anode displays a reversible capacity of 1225 mAh/g at 200 mA/g in the first cycle, and keeps a capacity of about 780 mAh/g as the current density gradually increases to 2.5 A/g, much higher than those of MS (678 mAh/g) and MS-PG (645 mAh/g) (Figure 4c). Moreover, when the current density returns back to 200 mA/g, the capacity of MS-CG increases to 1223 mAh/g, which is comparable to the initial capacity. Furthermore, after the impact of high current density at 2.5 A/g, the MS-CG still deliver rather stable cycling performance for 20 cycles with a capacity retention of about 94.4%, better than those of MS-PG (85.5%) and MS (81.9%). Besides, the MS-CG anode exhibits a high reversible capacity of 680 mAh/g after 250 cycles at 500 mA/g, corresponding to a capacity fading of only 0.17% per cycle, much lower than those of MS-PG (a

capacity fading of 0.57% per cycle in 150 cycles) and MS (a capacity fading of 0.59% per cycle in 150 cycles). The morphology of the MS-CG after 250 cycles was investigated by FESEM (Figure S5 in the Supporting Information). It is obvious that MoS₂ nanoflowers are obscure and only a few nanosheets are observed, implying that the capacity fading is due to the destruction of nanoflowers. The cycling stability of MS-CG is better than that of MS-PG, indicating the introduction of RGO during the growth of MoS₂ nanoflowers is more effective than the postintroduction to improve the electrochemical performance. The enhanced cycling performance of MS-CG is attributed to the crumpled RGO, providing efficient electronic transport network and facile efficient stress relaxation. The facile stress relaxation alleviates the structural destruction caused by the repeated volume change during cycling.³² The cycling stability of MS-CG is better than that of MS-PG, indicating the introduction of RGO during the growth of MoS₂ nanoflowers is more effective than the post-introduction to improve the electrochemical performance. Considering the carbon fiber may provide capacity, the electrochemical performance of carbon fiber cloth was carried out (Figure S6 in the Supporting Information). After subtracting the contribution from the carbon fiber cloth, the capacity of MS-CG is still much higher than the theoretical capacity of graphite.

Electrochemical impedance spectra (EIS) measurements of the MS and MS-CG before and after 10 cycles were carried out to evaluate the electrochemical kinetics (Figure 4d). The MS-CG before electrochemical cycling shows a low charge transfer resistance (R_{ct}), reflected by the small diameter of semicircle at the high-frequency region, which is much lower than that of the MS, confirming enhanced kinetics by the bicontinuous electronic conductive network. After 10 cycles, a new semicircle forming in the Nyquist plot of MS at the high frequency, which is assigned to the formation of SEI film with relevant resistance (R_f), but this is unobvious in the Nyquist plot of MS-CG.

Compared to carbon cloth-MoS₂ nanosheet composites,^{29,30} the MS-CG anode shows significantly enhanced cycling stability. The enhanced cycling stability is ascribed to the unique structural merits of MS-CG: (a) the carbon fiber restrains the agglomeration of nanoflowers;^{29,30} (b) the crumpled RGO and carbon fiber build a bicontinuous electronic transport network, improving the electronic conductivity;^{13,17} (c) the void spaces in crumpled RGO and the interstices among nanosheets ensure the effective stress releasing and volume buffering.³²

The crumpled RGO/MoS₂ nanoflowers on carbon fiber (MS-CG) have been synthesized via a facile hydrothermal method followed by heat treatment under H₂/Ar atmosphere. The bicontinuous electronic transport pathways and void spaces in the MS-CG are beneficial to the cycling stability. The MS-CG anode exhibits a high reversible capacity and excellent cycling stability. A high initial capacity (1225 mAh/g) of MS-CG is obtained at 200 mA/g. When cycled at 500 mA/g, the MS-CG anode displays a capacity fading of 0.17% per cycle in 250 cycles, which much better than that of MS and MS-PG. The high capacity and excellent cycling property make the MS-CG a promising anode for LIBs. This design also provides an efficient approach to enhance the cycling property of other electrode materials.

■ ASSOCIATED CONTENT

S Supporting Information

Detailed experimental section and additional Figure S1–S6. The Supporting Information is available free of charge on the ACS Publications website at DOI: 10.1021/acsami.5b02978.

■ AUTHOR INFORMATION

Corresponding Author

*E-mail: mlq518@whut.edu.cn.

Author Contributions

[†]F.X. and Z.C. contributed equally. The manuscript was written through contributions of all authors. All authors have given approval to the final version of the manuscript.

Notes

The authors declare no competing financial interest.

■ ACKNOWLEDGMENTS

This work is supported by the National Natural Basic Research Program of China (2013CB934103, 2012CB933003), the International Science and Technology Cooperation Program of China (2013DFA50840), the National Natural Science Fund for Distinguished Young Scholars (51425204), the National Natural Science Foundation of China (51272197), the Hubei Province Natural Science Fund for Distinguished Young Scholars (2014CFA035), the Fundamental Research Funds for the Central Universities (2013-ZD-7) and the Students Innovation and Entrepreneurship Training Program (WUT, 20141049701006). We are grateful to Prof. C. M. Lieber of Harvard University, Prof. J. Liu of Pacific Northwest National Laboratory and Prof. D. Y. Zhao of Fudan University for strong support and stimulating discussions.

■ REFERENCES

- (1) Tarascon, J.-M.; Armand, M. Issues and Challenges Facing Rechargeable Lithium Batteries. *Nature* **2001**, *414*, 359–367.
- (2) Dunn, B.; Kamath, H.; Tarascon, J.-M. Electrical Energy Storage for the Grid: A Battery of Choices. *Science* **2011**, *334*, 928–935.
- (3) Mahmood, N.; Zhang, C.; Hou, Y. Nickel Sulfide/Nitrogen-Doped Graphene Composites: Phase-Controlled Synthesis and High Performance Anode Materials for Lithium Ion Batteries. *Small* **2013**, *9*, 1321–1328.
- (4) An, Q.; Lv, F.; Liu, Q.; Han, C.; Zhao, K.; Sheng, J.; Wei, Q.; Yan, M.; Mai, L. Amorphous Vanadium Oxide Matrixes Supporting Hierarchical Porous Fe₃O₄/Graphene Nanowires as a High-Rate Lithium Storage Anode. *Nano Lett.* **2014**, *14*, 6250–6256.
- (5) Cao, K.; Jiao, L.; Liu, H.; Liu, Y.; Wang, Y.; Guo, Z.; Yuan, H. 3D Hierarchical Porous α -Fe₂O₃ Nanosheets for High-Performance Lithium-Ion Batteries. *Adv. Energy Mater.* **2015**, *5* DOI: 10.1002/aenm.201401421.
- (6) Mahmood, N.; Zhang, C.; Liu, F.; Zhu, J.; Hou, Y. Hybrid of Co₃Sn₂@ Co Nanoparticles and Nitrogen-Doped Graphene as a Lithium Ion Battery Anode. *ACS Nano* **2013**, *7*, 10307–10318.
- (7) Xu, Y.; Liu, Q.; Zhu, Y.; Liu, Y.; Langrock, A.; Zachariah, M. R.; Wang, C. Uniform Nano-Sn/C Composite Anodes for Lithium Ion Batteries. *Nano Lett.* **2013**, *13*, 470–474.
- (8) Wu, H.; Chan, G.; Choi, J. W.; Yao, Y.; McDowell, M. T.; Lee, S. W.; Jackson, A.; Yang, Y.; Hu, L.; Cui, Y. Stable Cycling of Double-Walled Silicon Nanotube Battery Anodes Through Solid-Electrolyte Interphase Control. *Nat. Nanotechnol.* **2012**, *7*, 310–315.
- (9) Raju, V.; Wang, X.; Luo, W.; Ji, X. Multiple Ambient Hydrolysis Deposition of Tin Oxide into Nanoporous Carbon To Give a Stable Anode for Lithium-Ion Batteries. *Chem.—Eur. J.* **2014**, *20*, 7686–7691.
- (10) Cai, Z.; Xu, L.; Yan, M.; Han, C.; He, L.; Hercule, K. M.; Niu, C.; Yuan, Z.; Xu, W.; Qu, L.; Zhao, K.; Mai, L. Manganese Oxide/

Carbon Yolk-Shell Nanorod Anodes for High Capacity Lithium Batteries. *Nano Lett.* **2015**, *15*, 738–744.

(11) Xiao, J.; Choi, D.; Cosimbescu, L.; Koech, P.; Liu, J.; Lemmon, J. P. Exfoliated MoS₂ Nanocomposite as An Anode Material for Lithium Ion Batteries. *Chem. Mater.* **2010**, *22*, 4522–4524.

(12) Yang, L.; Wang, S.; Mao, J.; Deng, J.; Gao, Q.; Tang, Y.; Schmidt, O. G. Hierarchical MoS₂/Polyaniline Nanowires with Excellent Electrochemical Performance for Lithium-Ion Batteries. *Adv. Mater.* **2013**, *25*, 1180–1184.

(13) David, L.; Bhandavat, R.; Singh, G. MoS₂/Graphene Composite Paper for Sodium-Ion Battery Electrodes. *ACS Nano* **2014**, *8*, 1759–1770.

(14) Hu, L.; Ren, Y.; Yang, H.; Xu, Q. Fabrication of 3D Hierarchical MoS₂/Polyaniline and MoS₂/C Architectures for Lithium-Ion Battery Applications. *ACS Appl. Mater. Interfaces* **2014**, *6*, 14644–14652.

(15) Liu, Y.; Zhao, Y.; Jiao, L.; Chen, J. A Graphene-like MoS₂/graphene Nanocomposite as a Highperformance Anode for Lithium Ion Batteries. *J. Mater. Chem. A* **2014**, *2*, 13109–13115.

(16) Zhang, C.; Wang, Z.; Guo, Z.; Lou, X. W. Synthesis of MoS₂-C One-Dimensional Nanostructures with Improved Lithium Storage Properties. *ACS Appl. Mater. Interfaces* **2012**, *4*, 3765–3768.

(17) Zhou, X.; Wan, L.-J.; Guo, Y.-G. Synthesis of MoS₂ Nanosheet-graphene Nanosheet Hybrid Materials for Stable Lithium Storage. *Chem. Commun.* **2013**, *49*, 1838–1840.

(18) Bindumadhavan, K.; Srivastava, S. K.; Mahanty, S. MoS₂-MWCNT Hybrids as a Superior Anode in Lithium-Ion Batteries. *Chem. Commun.* **2013**, *49*, 1823–1825.

(19) Zhou, X.; Wan, L.-J.; Guo, Y.-G. Facile Synthesis of MoS₂@CMK-3 Nanocomposite as an Improved Anode Material for Lithium-Ion Batteries. *Nanoscale* **2012**, *4*, 5868–5871.

(20) Bang, G. S.; Nam, K. W.; Kim, J. Y.; Shin, J.; Choi, J. W.; Choi, S.-Y. Effective Liquid-Phase Exfoliation and Sodium Ion Battery Application of MoS₂ Nanosheets. *ACS Appl. Mater. Interfaces* **2014**, *6*, 7084–7089.

(21) Ryu, W.-H.; Jung, J.-W.; Park, K.-S.; Kim, S.; Kim, I.-D. Vine-Like MoS₂ Anode Material Self-Assembled from 1-D Nanofibers for High Capacity Sodium Rechargeable Battery. *Nanoscale* **2014**, *6*, 10975–10981.

(22) Hwang, H.; Kim, H.; Cho, J. MoS₂ Nanoplates Consisting of Disordered Graphene-like Layers for High Rate Lithium Battery Anode Materials. *Nano Lett.* **2011**, *11*, 4826–4830.

(23) Xu, W.; Zhao, K.; Niu, C.; Zhang, L.; Cai, Z.; Han, C.; He, L.; Shen, T.; Yan, M.; Qu, L.; Mai, L. Heterogeneous Branched Core-Shell SnO₂-PANI Nanorod Arrays with Mechanical Integrity and Three Dimensional Electron Transport for Lithium Batteries. *Nano Energy* **2014**, *8*, 196–204.

(24) Luo, W.; Hu, X.; Sun, Y.; Huang, Y. Electrospinning of Carbon-Coated MoO₃ Nanofibers with Enhanced Lithium-Storage Properties. *Phys. Chem. Chem. Phys.* **2011**, *13*, 16735–16740.

(25) Gu, M.; Li, Y.; Li, X.; Hu, S.; Zhang, X.; Xu, W.; Thevuthasan, S.; Baer, D. R.; Zhang, J.-G.; Liu, J. In Situ TEM Study of Lithiation Behavior of Silicon Nanoparticles Attached to and Embedded in a Carbon Matrix. *ACS Nano* **2012**, *6*, 8439–8447.

(26) Ji, L.; Gu, M.; Shao, Y.; Li, X.; Engelhard, M. H.; Arey, B. W.; Wang, W.; Nie, Z.; Xiao, J.; Wang, C. Controlling SEI Formation on SnSb-Porous Carbon Nanofibers for Improved Na Ion Storage. *Adv. Mater.* **2014**, *26*, 2901–2908.

(27) Lin, J.; Peng, Z.; Xiang, C.; Ruan, G.; Yan, Z.; Natelson, D.; Tour, J. M. Graphene Nanoribbon and Nanostructured SnO₂ Composite Anodes for Lithium Ion Batteries. *ACS Nano* **2013**, *7*, 6001–6006.

(28) Jiang, J.; Li, Y.; Liu, J.; Huang, X.; Yuan, C.; Lou, X. W. D. Recent Advances in Metal Oxide-based Electrode Architecture Design for Electrochemical Energy Storage. *Adv. Mater.* **2012**, *24*, 5166–5180.

(29) Yu, H.; Zhu, C.; Zhang, K.; Chen, Y.; Li, C.; Gao, P.; Yang, P.; Ouyang, Q. Three-Dimensional Hierarchical MoS₂ Nanoflake Array/Carbon Cloth as High-Performance Flexible Lithium-Ion Battery Anodes. *J. Mater. Chem. A* **2014**, *2*, 4551–4557.

(30) Wang, C.; Wan, W.; Huang, Y.; Chen, J.; Zhou, H. H.; Zhang, X. X. Hierarchical MoS₂ Nanosheet/Active Carbon Fiber Cloth as a Binder-Free and Free-Standing Anode for Lithium-Ion Batteries. *Nanoscale* **2014**, *6*, 5351–5358.

(31) Cao, X.; Shi, Y.; Shi, W.; Rui, X.; Yan, Q.; Kong, J.; Zhang, H. Preparation of MoS₂-Coated Three-Dimensional Graphene Networks for High-Performance Anode Material in Lithium-Ion Batteries. *Small* **2013**, *9*, 3433–3438.

(32) Zhao, Y.; Feng, J.; Liu, X.; Wang, F.; Wang, L.; Shi, C.; Huang, L.; Feng, X.; Chen, X.; Xu, L.; Yan, M.; Zhang, Q.; Bai, X.; Wu, H.; Mai, L. Self-Adaptive Strain-Relaxation Optimization for High-Energy Lithium Storage Material Through Crumpling of Graphene. *Nat. Commun.* **2014**, *5*, 4565.

(33) Xie, J.; Zhang, J.; Li, S.; Grote, F.; Zhang, X.; Zhang, H.; Wang, R.; Lei, Y.; Pan, B.; Xie, Y. Controllable Disorder Engineering in Oxygen-Incorporated MoS₂ Ultrathin Nanosheets for Efficient Hydrogen Evolution. *J. Am. Chem. Soc.* **2013**, *135*, 17881–17888.

(34) Enyashin, A.; Ivanovskii, A. On the Capabilities of the X-ray Diffraction Method in Determining Polytypes in Nanostructured Layered Metal Disulfides. *J. Struct. Chem.* **2013**, *54*, 388–395.

(35) Li, H.; Zhang, Q.; Yap, C. C. R.; Tay, B. K.; Edwin, T. H. T.; Olivier, A.; Baillargeat, D. From Bulk to Monolayer MoS₂: Evolution of Raman Scattering. *Adv. Funct. Mater.* **2012**, *22*, 1385–1390.

(36) Chang, K.; Geng, D.; Li, X.; Yang, J.; Tang, Y.; Cai, M.; Li, R.; Sun, X. Ultrathin MoS₂/Nitrogen-Doped Graphene Nanosheets with Highly Reversible Lithium Storage. *Adv. Energy Mater.* **2013**, *3*, 839–844.

(37) Wang, L.; Xu, Z.; Wang, W.; Bai, X. Atomic Mechanism of Dynamic Electrochemical Lithiation Processes of MoS₂ Nanosheets. *J. Am. Chem. Soc.* **2014**, *136*, 6693–6697.

(38) Stephenson, T.; Li, Z.; Olsen, B.; Mitlin, D. Lithium Ion Battery Applications of Molybdenum Disulfide (MoS₂) Nanocomposites. *Energy Environ. Sci.* **2014**, *7*, 209–231.

(39) Wan, J.; Bao, W.; Liu, Y.; Dai, J.; Shen, F.; Zhou, L.; Cai, X.; Urban, D.; Li, Y.; Jungjohann, K. In Situ Investigations of Li-MoS₂ with Planar Batteries. *Adv. Energy Mater.* **2014**, *5* DOI: 10.1002/aenm.201401742.

(40) Xiao, J.; Wang, X.; Yang, X. Q.; Xun, S.; Liu, G.; Koech, P. K.; Liu, J.; Lemmon, J. P. Electrochemically Induced High Capacity Displacement Reaction of PEO/MoS₂/Graphene Nanocomposites with Lithium. *Adv. Funct. Mater.* **2011**, *21*, 2840–2846.

(41) Ji, X.; Lee, K. T.; Nazar, L. F. A Highly Ordered Nanostructured Carbon-Sulphur Cathode for Lithium-Sulphur Batteries. *Nat. Mater.* **2009**, *8*, 500–506.

(42) Ding, S.; Zhang, D.; Chen, J. S.; Lou, X. W. D. Facile Synthesis of Hierarchical MoS₂ Microspheres Composed of Few-Layered Nanosheets and Their Lithium Storage Properties. *Nanoscale* **2012**, *4*, 95–98.